2023 IEEE/ASME International Conference on Advanced Intelligent Mechatronics (AIM)
June 28-30, 2023. Seattle, Washington, USA

Alternative Locomotion Modalities for Lunar Rover

Naphasthanan Phornpimonchoke, Sittiphol Koosermmit, Ashira Tanakijchumroon, and Ronnapee Chaichaowarat, *Member, IEEE*

***Abstract*—Interplanetary exploration is at its prime since space transportation technology has become more convenient than ever. Our moon is the primary candidate to become the first extraterrestrial base of space flight operations in the future. The rocker bogie wheel design has been the standard design of locomotion modality for exploration rovers. It could navigate lunar regolith terrain but does not perform well on steep slopes and has the tendency to get permanently stuck on granular media. Alternatively, a legged rover design which contains more degree of freedom joints could free itself when become stuck and could navigate slopes more safely. This paper contains the process of designing and experimenting on an alternative locomotion modality for lunar regolith which could adapt to navigate up and down sloped terrains. In addition, the design would also allow for transformation into roll mode to travel downhill which would optimize energy consumption throughout different types of encountered terrains.**

I. Introduction

Humanity has always been stepping forward in technological advancement, and through scientific and mathematical knowledge, we were able to reach out beyond our own planet. Energy efficiency and reliability are major design concerns for operating an unmanned machine on distant planetary bodies. The key challenge of this paper is to design, fabricate, and conduct experiments on a legged rover design which serves as an alternative non-conventional locomotion method for navigating off-world regolith terrains.

We gathered information from different sources to find out which configuration is the most suitable. The standard locomotion modality of a lunar rover is rocker bogie design [1]. This is a reliable rigid suspension system but could be prone to compromising wheel slips [2] because the system is passively fixed. This is why an alternative design is developed and analyzed in this paper. Autonomous quadrupedal robot "Spot" by Boston Dynamics [3] was meant for operation in challenging terrain usually inaccessible by wheeled robots. This technology aims to improve navigation on difficult terrains and mission performance. Hybrid wheeled-leg rover "Sherpa" is quadrupedal rover, each leg comes with a powered wheel at the tip. The design is superior to a passive suspension system because it can release itself from getting stuck. The active suspension comes with a higher operation cost but allows much more maneuverability and configurations [4]. The MorpHex MKII is a robot which can transform into many shapes including a sphere [5], and the customizable design of RHex hexapedal robot is especially interesting for testing different specialized legs and future development [6].

N. Phornpimonchoke, S. Koosermmit, and A. Tanakijchumroon were with the International School of Engineering, Chulalongkorn University, Bangkok 10330, Thailand. R. Chaichaowarat is with the International School of Engineering, Chulalongkorn University, Bangkok 10330, Thailand (e-mail: ronnapee.c@chula.ac.th). The authors contributed equally to this work.

The main inspiration for this paper comes from "Bionic Wheel Bot" created by Festo, which mimics the movement of a cartwheeling spider (Cebrennus rechenbergi) [7]. The design allows configuration change for movement optimization. On level surfaces, rolling is advantageous and allows twice the speed compared to walking configuration. When the ground is uneven, walking is more efficient. It could navigate up to 5% inclined surface. The team weighs the advantages and drawbacks of each design before combining the ideas into a new original design. The construction, and aspects for evaluation are inspired by [8] but the design in this paper will be focused on application on lunar terrain. The reconfigurable robot from the reference uses terrain compression movement to navigate on solid ground, while the design for this paper only transforms to roll downhill as means of conserving energy when traveling down craters. The study of sensitive dependence of legged rover on granular media was mentioned in [9]. Another study about the resistive force on the granular media also presented the design concept for simplifying motor control [10] and studied the movement on sandy terrain. The design with hybrid leg-wheel configuration was presented in [11] for testing the active suspension system on regolith terrain. The method for optimizing movement on slopes used for the flipper-driven design [12] is also applied to this study.

The final design is a four-legged rover that can walk up slopes and transform into cylindrical shape for rolling down hills in hopes to save energy. Three prototypes have been created throughout different aspects of the design process along the way. The scope of calculations and test results in this paper will only account for the latest prototype design which could navigate up to 36° of slope, which lies in the typical slope angle of lunar south pole crater [13]. In the end, the final results passed the requirements for the objective which means the legged rover design is viable as an alternative locomotion modality for lunar rover.

This paper is organized as follows: Section II describes the design method along with simulation results. Section III presents the prototype of the legged rover and describes the experimental setup. Section IV discusses the results while section V summarizes the key findings and suggests for continuation of this paper.

II. Design Process

A. Design Principal

This paper aims to combine different ideas from research to innovate alternative locomotion beneficial for navigating near the crater surface at the south pole of the Moon. The rover should be able to navigate soft regolith terrain while being on a slope, which has not been fulfilled by any of the researched technologies. The final rover design should fulfill all requirements and be practical for real use when scaled up to

actual size. Walking gait movement has been selected due to the high DOF, and transformation of legs aims to increase energy efficiency while travelling downhill. The C-shape foot has been chosen based on [14] since its morphology allowed leg elements to reach deeper depths and access larger stress regions, thus creating efficient forward motion. The modular design allows for rapid prototyping and specific component experiments.

B. Maximum Torque Determination

The analysis will be described in this section confirms that the maximum load of the design given by the posture and dimension of the rover itself will not exceed the maximum torque that the motor can withstand. Of all movements the rover needs to perform, there is a posture that exerts the highest torque to a specific motor. The kinetics of the rover in the mentioned posture are analyzed based on the side viewed diagram, shown in Fig. 1. The posture is when the rover lifts two legs located diagonally opposite to each other up and leaves the two other legs standing on the ground while having same angle θ_1 and θ_2. Since the figure is symmetric about the y-axis, only the left half of the rover is analyzed. By applying the Newton's laws of motion, the torque T_1 at motor-D1 and the torque T_2 at motor-D2 are related to the physical parameters and variables including the radius of rover body R, the body weight mg, the friction f, the length of the foot l_1, the length of the thigh l_2, the angle of the foot relative to the ground θ_1, the angle of the thigh relative to the ground θ_2, via (1) and (2) respectively.

$$T_1 = f l_1 \sin\theta_1 + \frac{mg l_1 \cos\theta_1}{2} \quad (1)$$

$$T_2 = f l_1 \sin\theta_1 + \frac{mg l_1 \cos\theta_1}{2} + \frac{mg l_2 \cos\theta_2}{2} + f l_2 \sin\theta_2 \quad (2)$$

The trial-and-error process is required to relate the unknown design parameters (input) with the amount of torques required at the motor-D1 and the motor-D2 via the known parameters and variables. The input parameters are the foot length, the thigh length, the foot angle relative to the ground, and the thigh angle relative to the ground. The computed motor torques are compared to the 0.8 N·m torque limit computed from the motor's stall torque of 1.4 N·m with the safety factor of 1.7. The input parameters were adjusted until the torques of both motors satisfied the torque limit to confirm that the rover can transform into the cylindrical shape for the rolling configuration, as shown in Fig. 2. According to the designed parameters of the rover prototype, as shown in Table I, the torques T_1 of 0.29 N·m and T_2 of 0.71 N·m are required for the motor-D1 and the motor-D2 respectively.

C. Cost of Transport Comparison

The cost of transport COT is employed to compare the transportation modes between walking and rolling by considering the power P and the body velocity v_{body}.

$$COT = \frac{P}{mg \cdot v_{body}} \quad (3)$$

For both walking and rolling, the body weight mg is assumed to be the same. Therefore, the power and the body velocity are the only two parameters affecting the COT. For simplicity of calculation, a few assumptions were made as follows: The

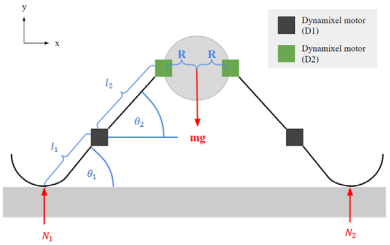

Fig. 1. Side-viewed diagram shows forces and parameters for estimating motors' torques in the two-leg standing posture.

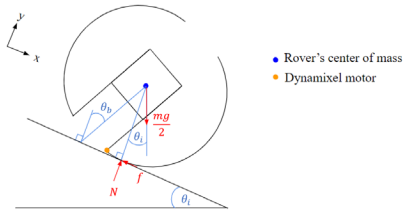

Fig. 2. Side-viewed diagram shows forces and parameters for estimating motors' torques in the rolling configuration.

TABLE I. DESIGNED PARAMETERS OF THE ROVER PROTOTYPE

Parameter	*Value*	*Unit*
Thigh length	60	mm
Foot length	105	mm
Thigh angle relative to the ground	40	deg
Foot angle relative to the ground	90	deg
Total mass of the rover	1.40	kg

rover curls into a perfect circle. The center of gravity is located at the center of the circle. The two motors in each leg and the tip of the leg lie on the same line perpendicular to the ground at the initial position.

First, the power draw of rolling configuration is elaborated. According to the motor's e-manual, torque and current are directly proportional, while power increases proportionally with current drawn as shown in (4), where I is current, and V is voltage. Thus, power increases proportionally with torque. The torque T_1 and T_2 are related to the physical parameters and variables, via (5) and (6) respectively. The equations were derived to monitor torque of each motor in static condition of the rover in rolling configuration Fig 2.

$$P = VI \quad (4)$$

$$T_1 = R\left(\left(\frac{mg}{2}\sin\theta_i\right)(1-\cos\theta_b) - \left(\frac{mg}{2}\cos\theta_i \sin\theta_b\right)\right) \quad (5)$$

$$T_2 = T_1 + \frac{mg}{2} l_2 \sin(\theta_i + \theta_b) \quad (6)$$

The amount of torques required during the transition stages are the functions of the angle of the inclined plane θ_i and the angle of the rover's body relative to the ground θ_b. The equations show that from 0° to 36° (the maximum slope of the crater [13]) the maximum torque is observed at 0°. Therefore, the angle of the inclined plane is fixed at 0°. By varying the angle of the rover's body relative to the ground from 2° to 178°, the torques required from the two motors are plotted, as shown in Fig. 3. The maximum and the average torque of the motor-D1 are 0.76 and 0.49 N·m whereas that of the motor-D2 are 0.55 and 0.35 N·m, respectively. While rolling, only two out of four legs are touching the ground and have the total average torque of 1.68 N·m (or (0.49 + 0.35 N·m) × 2 legs).

Considering the walking motion of the rover mentioned in the previous section, the static case while the rover is standing with its two legs is the scenario that generates torque less than the lowest amount of torque created on each motor in the normal walking condition and used to compare with the average torque during the rolling. The torque in the mentioned scenario has already been calculated in the previous section, where the total torque is 2 N·m (or (0.29 + 0.71 N·m) ×2 legs).

In conclusion, posture with the lowest torque of the walking configuration still creates a greater amount of torque than the average torque during rolling. This means the power drawn from rolling is much lower than walking, while the body velocity when rolling downhill is expected to be faster than walking downhill. Combining the results that rolling has greater velocity and lower power drawn, the COT of the rolling is much lower than walking which is desirable for lunar application.

D. Foot Drag Determination

For the robot to successfully travel on granular media, the foot that anchors on the sand as other feet are stepping forward should not simply slip through the sand. According to [6], robot traveling in granular media can transition from walking to swimming stage when reached a certain threshold, rendering it almost stationary, like wheels of a car spinning uselessly as it essentially digs the car downward instead of traveling forward. Therefore, the objective of foot geometry design aims to maximize the drag created by the foot when moved horizontally. The feet that are propelling the robot forward, as four different designs shown in Fig. 4, were simulated via *ANSYS Fluent* by varying two features: presence of holes and rib sizes.

The simulation results are compared, as the plots in Fig. 5. The difference of drag force is more noticeable at the higher speed. Both the augmented ribs and the holes each contributes to the higher drag. This could be because of the internal surface of the hole that is normal to the sweeping direction of the foot, thus creates an extra drag. The configuration with the highest drag is chosen for the prototype. Drags at the speed 0.216 m/s are approximately 4 – 6 times higher than that of the speed 0.056 m/s. At the higher speed, the effect of holes or modified ribs alone increases the drag force about 50%. The combination of the holes and modified ribs raises the drag by almost 80%. At the lower speed, the presence of holes or modified ribs alone does not significantly alter the resultant drag but the combination of both features results in almost up to 25% increase in drag.

The combination of holes and modified ribs has the highest positive impact on drag. This desirable characteristic is more prominent at higher speed. However, it is to be noted that the accuracy of these simulations is not prioritised since only the features are the only varying parameters, not the dimension of the features themselves. The necessary output from the simulation is the general trend of the result. Additionally, holes have another advantage in terms of the overall efficiency of the robot that is not investigated in this simulation. That is, it allows the granular media to fall through, avoiding carrying extra unnecessary media weight along with the robot.

Considering the CFD simulated results, the final design of

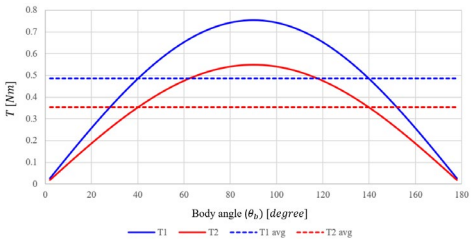

Fig. 3. Motor torques varying against the angle of rover's body relative to the ground at zero degree of the slope.

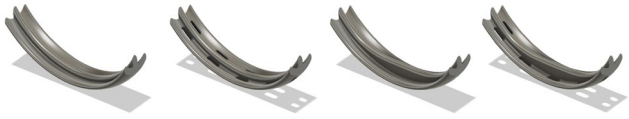

Fig. 4. Candidate models for foot drag determination: (a) Constant rib no holes, (b) Constant rib with holes, (c) Modified rib no holes, and (d) Modified rib with holes.

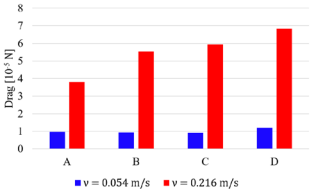

Fig. 5. Foot drag results: (A) Constant rib no holes, (B) Constant rib with holes, (C) Modified rib no holes, and (D) Modified rib with holes.

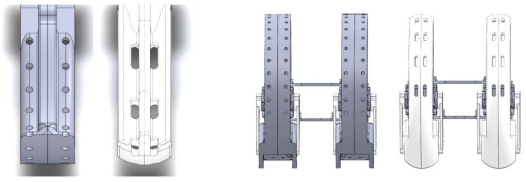

Fig. 6. The previous (left) and the new (right) foot designs.

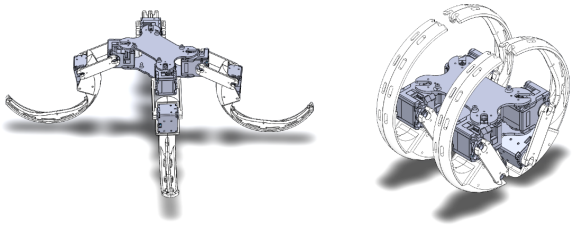

Fig. 7. CAD rendering of the rover prototype in the standing and the rolling configurations.

the foot was determined, as shown in Fig. 6. The flat surface of each foot has been replaced with curved surface. The rib section has been changed from constant profile to varied profile to maximize the foot drag on the gait direction. Fewer connection points are provided, which makes the foot profile more accurate for the CFD model. The motor connection area, see Fig. 7, has been fortified for simpler assembly and increased robustness.

III. Prototype and Experimental Setup

The rover protype, see Fig. 8 (a), was built from 3D printed PLA. Each of the legs contains: the foot section actuated by a 1-DOF motor, and the thigh section actuated by a 2-DOF motor connecting each leg to the electronic compartment. The foot section is manufactured from two separate components screwed together to form the ideal shape analyzed by the CFD process. The thigh section consisting of two separate pieces is

located between the 1-DOF and the 2-DOF motors to allow height variation movement. See Fig. 8 (b), the electronic compartment is the central module connecting all the legs together while holding the circuits and the power source (11.1 V 1.3 mAh LiPO battery). The ROBOTIS OpenCM 9.04 microcontroller board is used along with the RS485 expansion board to provide adequate power output for all the motors. The 2-DOF Dynamixel 2XL-430-W250-T is selected for driving the thigh whereas the 1-DOF Dynamixel XL-430-W250-T is used for driving the foot.

Aiming to determine and analyze the performance and efficiency of the robot, it will be tested for body velocity, torque applied at each motor, power, and energy consumption. These values are measured when the robot is ascending a slope of granular media with slope angle of 0°, 10°, and 20 ° at varying speed, as well as descending the 20° of slope with walk and roll mode. The ascending experiment aims to study the influence of different gait speed and slope angle θ on the walk mode characteristics. The gait speed is varied by gait scaling labeled as 0.5, 1, and 2 which represents scaling of the speed, referred to the motor's yawing and pitching rotational speeds of 1.44 rad/s. Meanwhile, the descending experiments are mainly done to compare the efficiency of roll and walk mode. The experiment was conducted as the setup shown in Fig. 9, where the body velocity is measured through the measuring tape in conjunction with the video camera, while the rest of the data collected were acquired via laptop connect to the robot during the experiment. This includes the motor torque relating to the current, the power obtained by inputting the acquired torque value on to a performance graph provided by the manufacturer of the motor, and the energy consumption which is calculated from average power and body velocity.

The robot performs walk and roll modes following predetermined commands embedded on-board, specifying the routine with the fixed set of angular velocities for each sample. At the end of roll mode, the robot spreads its legs out of its cylindrical form and comes to a stop at the end of the slope to imitate a realistic representation of power and energy consumption.

IV. Results and Discussion

A. Body Velocity

As the slope angle increases, the body velocity decreases, approaching zero across all gait speed, as illustrated in Fig 10. The body velocity also increases at higher gait speed at all slope angles. This indicates that using higher gait velocity at ground level is more efficient than lower gait velocity. Increase in gait scaling from 1 to 2 results in body velocity with higher than two times growth. This implies that the relationship between body velocity and gait velocity is not only nonlinear but also has a threshold where the higher gait velocity would result in significantly greater body velocity at the slope angle lower than the certain value. Additionally, it is observed that the higher gait speed, the more body velocity drops as slope angle raises.

B. Torque

To study the effect of slope angle on torques experienced by the motors, ones at joints connecting thigh to the body of the robot on varying slope angle are shown in Fig. 11. This includes the torque in two directions, yaw and pitch, however,

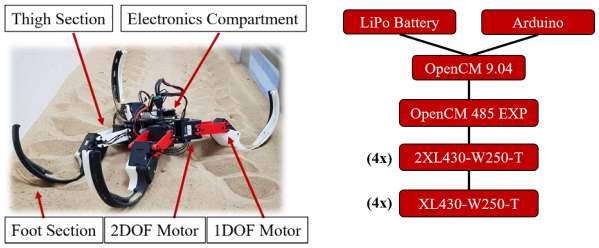

(a) (b)

Fig. 8. (a) The built prototype of the four-legged rover. (b) Detailed electronic diagram shows the hardware connection.

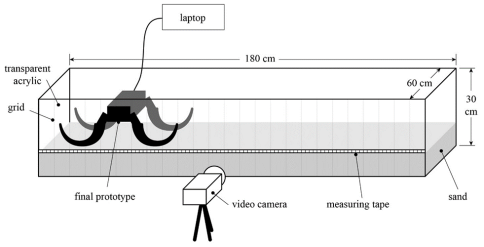

Fig. 9. Schematic shows the experimental setup.

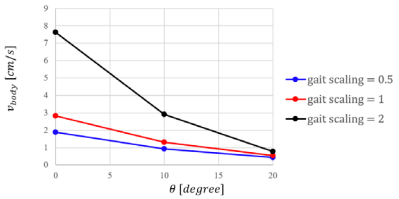

Fig. 10. Body velocity varies with the slope angle tested at different speeds.

only those of right legs are illustrated as the robot is assumed to be symmetrical. Torque on all cases peaked periodically and in line with the sweeping motion that propels the robot forward where both pitch and yaw torques rapidly increase every 3.5 seconds. Each peak remains relatively high for at most 2 seconds before dropping. It is followed by peaks of the left leg where the graphs would be similar in characteristics but shifted by 1.75 seconds (half of the peaking period).

As the slope increases, the pattern of periodic peaks remains the same but generally increases in magnitude in all cases except for the pitching torque on front leg where torque at $\theta = 0°$ is mostly higher. The increase in yawing torque is due to weight that shifted to the rover's vertical axis, $mg\sin\theta$. Meanwhile, the pitching torque decreases on front legs but heightens on back legs because the center of gravity shifts backwards as slope angle increases, causing more weight originally carried by the front legs to be distributed towards the back. The increment in slope angle also affects other aspects of the torque magnitude. For example, for yawing torque of front leg, the torque fluctuates as it rapidly increases then drops down rapidly at 0° slope angle but rises smoothly and remains at peaks for approximately 1 second for higher slope angles.

On the other hand, the pitching torque of front legs at 0° slope is much larger than that at higher slope angle. Its characteristics is almost that of square wave as it remains at 3.5 N·m for roughly 2 seconds and drops down to almost 0 N·m for another 2 seconds. Meanwhile, torque at the knee, where the motor is kept at fixed position, is minimal and swings from 0 to 0.1 N·m. This characteristic of the torque at the knee remains for all the angles of slope and are omitted in the figures.

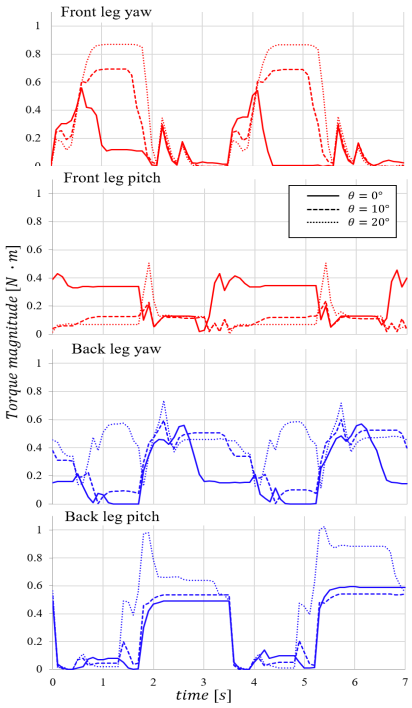

Fig. 11. Torque of each joint varying against time during ascent using the walking mode, tested at different slopes.

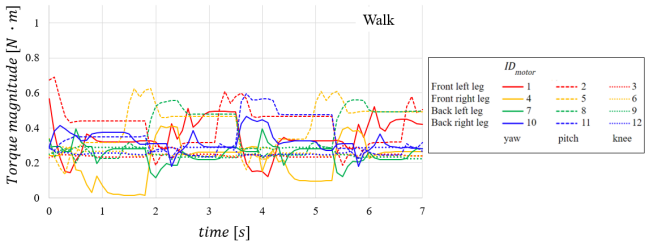

Fig. 12. Torque of each joint vary against time during descent, tested at 20° slope for the walking mode.

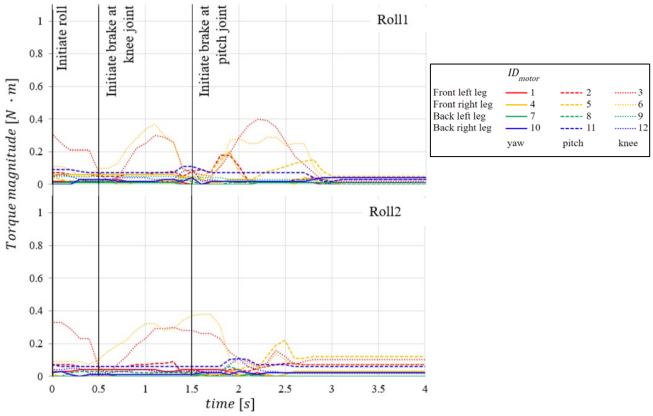

Fig. 13. Torque of each joint vary against time during descent, tested at 20° slope for the rolling mode.

To compare walk and roll mode, both were studied on a 20° slope. While the case with walk mode down the slope angle of 20° is an average from all samples, as shown in Fig. 12, different samples from roll mode were determined to be analyses separately as shown in Fig. 13. This is because the robot was expected to roll down the incline naturally without human interference. However, that was not the case as the robot unexpectedly stays perfectly still. This is likely due either or the combination of the low center of gravity of the robot itself relative to the center of the circle cross-section created by its foot, the shape of the robot in roll mode which is not perfectly circular, and the shifting of the sand as the robot sinks in from its own weight. Therefore, for each rolling sample, the initial velocity of the robot is likely slightly different as it was not initially designed in the experimental method. As shown in the Fig. 12, the graph of walk mode down the 20° of slope is highly irregular. Compared to ascending, the torque at all motor ID while descending generally flattens and shifts up for about 0.3 N·m. This means that although there are less peaks, there is a constant baseline torque due to the shift.

Furthermore, the peaking pattern observed from previous cases seems to also shift regarding to time by half a period (or 3.5 s). For the rolling mode, also executed at slope of -20°, it can be seen that the torque at the knee of front leg increases at the initiation of break. The main difference between the two roll cases is the number of peaks in torque at the front knees. This is due to the initial velocity that affects the angle of rotation where the brake starts. It is hypothesized that in the first roll case (roll1), the robot had rolled slightly farther when the brake is initiated. This results in inadequate friction, leading to the robot continuing to roll. Nevertheless, the combination of position of center of gravity and residual velocity allows the robot to roll backward with the force of its own weight and comes to a stop. In the second case (roll2), however, the brake initiated earlier in the roll, which results in sufficient friction or drag that allows the robot to decelerate and comes to a stop. It is to be noted that at the beginning of the roll, the torque applied by the motor at the knee of the front left leg to stay stationary in roll position is significantly lower than every other joint. This is likely due to human intervention necessary for initiating the rolling motion.

C. *Power Consumption*

According to the plots in Fig. 14, the power consumption trends are similar for all three slopes where the peak indicates motion when two of the legs were sweeping and that the front leg experienced drag in yaw direction while back leg experienced drag in both yaw and pitch direction. The crest of the graph indicates when the rover places all the legs on the sand which is reasonable since all of the joints are stationary. It is obvious in the graph that the rover consumes more power as the slope keeps increasing, this was because of the gravitational component and the excessed drag from sand on the back leg that was created by the front leg. Surprisingly, the increasing trend of the average power consumption as slope angle increases is relatively linear. Additionally, the peaks in power consumption of the two lower slope angles are approximately the same, while that of slope angle of 20° is noticeably different.

For ascending, the average power consumption is less than that at 0° slope. This means that gravity helps the rover to walk downhill more efficiently. However, the average power consumption of walk mode is still significantly greater than that of the rolling mode and it even took much longer time to finish the distance of 1 m. This is in line with the prediction made in the design process. For both rolling trials, it can be seen in the plots that the power consumption rises after a second, this happened because the rover needs more power to neutralize its momentum or to stop itself.

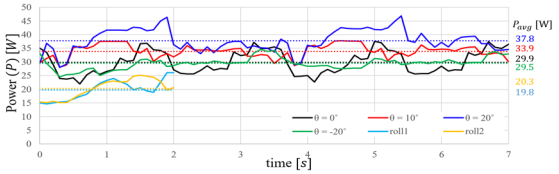

Fig. 14. Power consumption varies with slope angle tested at varing speeds.

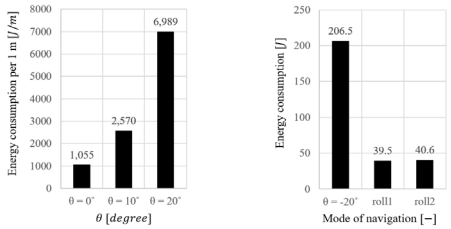

(a) (b)

Fig. 15. (a) Energy consumption per distance by walking mode at different inclined angles. (b) Energy consumption for descending the 20° slope.

D. Energy Consumption

When ascending the slope, the energy consumption of the robot increases exponentially as the slope increases, as shown in Fig. 15 (a), this is because not only that the motor needs to provide more torque against gravity as slope increases, but the motor also needs to operate longer to achieve the same distance. This is because the rover was having a hard time climbing high slopes, since the gait has not been optimized in this paper. The longer the motors operate, the higher the energy consumption, since the energy is calculated from time integral of the power consumption. Fig. 15 (b) demonstrates the energy consumption for the rover to descend the slope of 20° for a distance of 1 meter. As shown in the plot, walking down the slope consumes much greater energy than rolling down the slope. This confirms the theoretical calculations in the design section.

V. Conclusion

From the objective of the paper, which is to design an innovative non-conventional rover locomotion concept and do a relevant test on a prototype, the paper achieved most of the quantitative and measurable requirements. The four-legged walking rover could navigate the slopes up to 36° and transform to roll down a slope. The detailed design through CFD and additive manufacturing of rover leg has resulted in a compact but robust design proven viable for navigating fluffy lunar regolith terrain effortlessly. The design could achieve an average velocity up to 0.8 m/s when climbing up a 20° slope of fluffy granular media. Increases in gait speed exponentially increases the body velocity. Body velocity also drops significantly as slope angle increases. The roll mode is proven to be more efficient in terms of power consumption, which is significantly higher in walk mode. When walking, as slope angle increases, power consumption increases while speed decreases. In conjunction with the slope angle and gait velocity, this suggested that there could be a certain gait speed that contributes to minimum COT at certain slope angle.

The transformable four-legged rover is scalable which should allow for better torque to weight ratio to carry more load, climb with higher body velocity or better power consumption rates. With newfound excess torque, the rover body could even be designed to carry scientific tools or heavy payloads. The results from foot drag analysis via CFD, that only prioritize on the varying parameters, can also be used as baseline information along with extra simulations in the future to accurately optimize number/size of holes and ribs. Overall, this paper has achieved most of the set goals and shines a path for a new type of efficient interplanetary rover to navigate regolith terrains and pave the way to new discoveries previously intangible to mankind. It is to be noted that there are several factors of lunar environment that are not presented in the experiments. The most substantial of which is the gravity which would affect the motor's torque and the robot's interaction with the granular media.

Acknowledgment

This research project is partly funded by Tronormos Co., Ltd., Bangkok, Thailand.

References

[1] B. D. Harrington and C. Voorhees, "The challenges of designing the rocker-bogie suspension for the mars exploration rover," in *Proc. Aerospace Mechanisms Symp.*, pp. 1–12, 2004.

[2] R. Chaichaowarat and W. Wannasuphoprasit, "Wheel slip angle estimation of a planar mobile platform," in *Proc. Int. Symp. Instrumentation, Control, Artificial Intelligence, and Robotics*, pp. 163–166, 2019.

[3] Boston Dynamics, "Spot® - The Agile Mobile Robot", Available: https://www.bostondynamics.com/spot [Accessed: Feb-2023].

[4] F. Cordes, et al., "An active suspension system for a planetary rover," in *Proc. Int. Symp. Artificial Intelligence, Robotics and Automation in Space*, pp. 1–7, 2014.

[5] K. Halvorsen, "MorpHex MKII", Available: http://zentasrobots.com/robot-projects/morphex-mkii/ [Accessed: Apr-2023].

[6] U. Saranli, M. Buehler, and D. E. Koditschek, "RHex: A simple and highly mobile hexapod robot. *Int. J. Rob. Res.*, vol. 20, no. 7, pp. 616–631, 2001.

[7] Festo Coporation, "BionicWheelBot", Available: https://www.festo.com/us/en/e/about-festo/research-and-development/bionic-learning-network/highlights-2018/bionicwheelbot-id_32767/?siteUid=fox_us&siteName=Festo+USA [Accessed: Feb-2023].

[8] T. Nemoto, R. E. Mohan, and M. Iwase, "Rolling locomotion control of a biologically inspired," *J. Robot.*, pp. 1–10, 2015.

[9] C. Li, P. B. Umbanhowar, H. Komsuoglu, D. E. Koditschek, and D. I. Goldman, "Sensitive dependence of the motion of a legged robot on granular media," *PANS*, vol. 106, no. 9, pp. 3029–3034, 2009.

[10] C. Li, G. Zhang, and D. I. Goldman, "A resistive force model for legged locomotion on granular media," *Adaptive Mobile Robotics*, pp. 433–440, 2012.

[11] S. Shrivastava, et al., "Material remodeling and unconventional gaits facilitate locomotion of a robophysical rover over granular terrain," *Science Robotics*, vol. 5, no. 42, 2020.

[12] N. Mazouchova1, P. B. Umbanhowar, and D. I. Goldman, "Flipper-driven terrestrial locomotion of a sea turtle-inspired robot," *Bioinspir. Biomim.*, vol. 8, pp. 1–14, 2013.

[13] R. V. Wagner, M. S. Robinson, E. J. Speyerer and P. Mahanti, "Topography of 20-km Diameter Craters on the Moon," Available:https://www.lpi.usra.edu/meetings/lpsc2013/eposter/2924.pdf. [Accessed: Feb-2023].

[14] C. Li, T. Zhang, and D. I. Goldman, "A terradynamics of legged locomotion on granular media," Science, vol. 339, no. 6126, pp. 1408–1412, 2013.